Ocean Swell Evolution Study with Buoys and Synthetic Aperture Radar

Antony K. Liu[1], David W. Wang[2], Hsuan. S. Chen[3]
[1] NASA/Goddard Space Flight Center
[2] Computer Sciences Corporation
[3] NOAA/National Weather Service

Abstract

This study examines the capability of spaceborne synthetic aperture radar (SAR) imagery to track a wave field generated by an intense storm in the northeast Pacific over a several day period. The ERS-1 SAR imagery is compared with NDBC (National Data Buoy Center) buoys. Hindcast results from the numerical wave model are also used for comparisons. The SAR spectra were largely linear in this case, which is related to the orientation of the satellite orbital track. That is, the east-west traveling swells are range-traveling waves. By using a wave kinematic model, the swell field generated by storm can be tracked over a four day period as observed by SAR and NDBC buoys. The difference in the arrival times of the swells between the buoy stations and the SAR scenes along the coast clearly indicated the feasibility of the advanced warning of high swell. This application for storm tracking and coast watch could be crucial to the safety of offshore operations.

1. Introduction

The tracking of storms and their associated wave field is of interest, both scientifically, in terms of air-sea interaction problems and wave models, and operationally, for monitoring potential hazardous conditions for shipping routes and coastal environments. Early studies showed that waves could be accurately identified as emanating from storms thousands of kilometers away. Waves generated from severe storms approaching landfall clearly can lead to potentially dangerous conditions for coastal inhabitants. Established networks of wave buoys, usually relatively close to shore, with synthetic aperture radar (SAR) imagery can provide valuable and near-real time information for coastal monitoring.

SAR imaging of surface gravity waves in the ocean has been demonstrated by many investigators, although the relative importance of imaging mechanisms such as hydrodynamic modulation, tilt modulation, and velocity bunching is still not that well understood (Alpers et al., 1981; Hasselmann et al., 1985). However, for ocean swell, the SAR imaging mechanism is linear in general and the resultant wave spectra are accurate, at least in terms of wavelength and direction. A range of studies has demonstrated the utility of SAR wave imagery for examining the evolution of wave fields (Liu and Peng, 1993; Peng and Liu, 1995), and studying wave-current interactions (Liu et al., 1994).

2. SAR Observations of Ocean Waves

Using ERS-1 high resolution SAR data (25 m resolution) from the Gulf of Alaska, a 6 km * 6 Km subscene is selected with dc bias removed, cosine-edge weighted and then the SAR data is two-dimensional fast Fourier transformed to obtain the wave number spectrum. Figure 1a shows the SAR spectrum collected on November 2, 1991 in the Gulf of Alaska with peak wavelength of 223.5 m and propagation direction of 274° from the North. To validate and to calibrate the wave spectrum derived from SAR data, the in-situ buoy data from the National Data Buoy Center (NDBC) and the hindcast results of numerical wave model from National Meteorological Center are used as shown in Figure 1b (WAMDI Group, 1988). The buoy and wave model results show the peak wave period of 12.5 sec (corresponding to a wavelength of 244 m) and propagation direction of 280° from the North. For the dominant wave component, the SAR spectrum compares reasonably well with the buoy and model results. However, the SAR spectral shape is distorted by the radar transfer function as compared to model results.

A typical Alaska SAR Facility wave product collected on December 29, 1991 in the Gulf of Alaska is shown in Figure 2 with a SAR subscene in the left panel and a SAR spectrum in the right panel. This large swell system of 531.5 m wavelength was also observed from the NDBC buoy data with 4 m significant wave height. An assessment of the measurement accuracy of SAR-derived wavelength and direction was performed using comparisons with NDBC buoy data sets over varying environmental conditions. Figure 3 shows the comparison of SAR-derived wavelength and buoy wave period with the deep water dispersion relation (solid curve). The data with date in 1991 (indicated by cross)

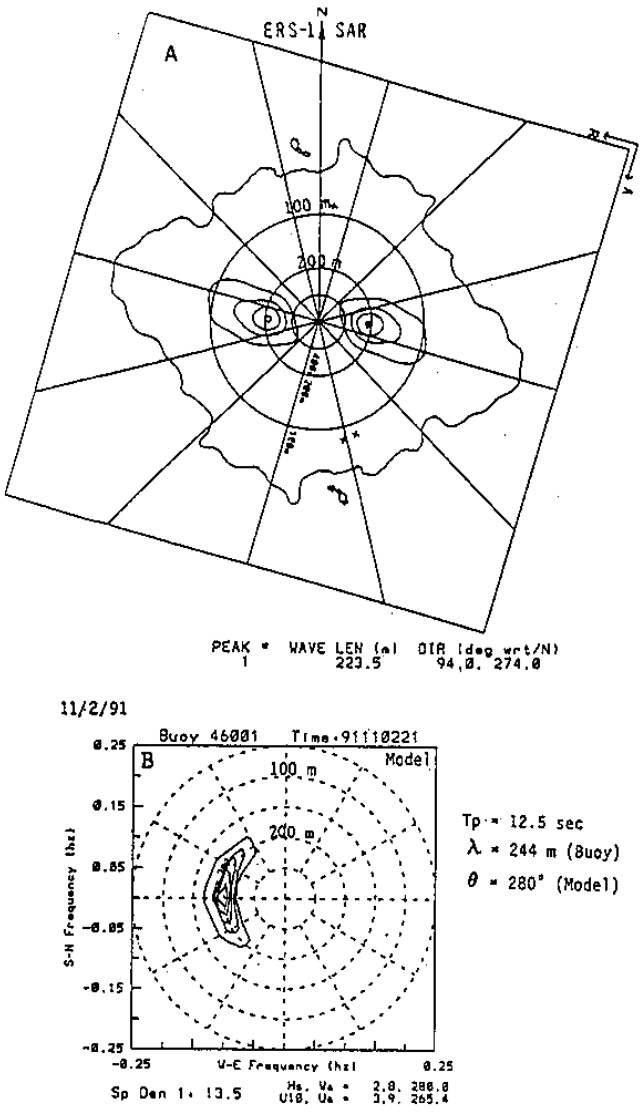

Figure 1. Comparison of (a) ERS-1 SAR spectrum, (b) Buoy data, and Wave Model Results from November 2, 1991 in the Gulf of Alaska.

are from ERS-1, and three data with circles are from JERS-1. As shown in the comparisons, the SAR-derived wavelength agrees with the buoy data within 10%. The comparisons of SAR-derived wave directions with the numerical results show an agreement within 15 degree. In summary, SAR wave spectra derived using a simple filter and no transfer functions were found to be reasonably accurate in measurements of wavelength and direction. This was largely fortuitous due to the meteorological conditions found in the northeast Pacific from September to December, 1991, where east-west swell (range traveling relative to the ERS-1 flight path) were predominantly measured. Thus, under favorable conditions, these products can be reliably used for investigation. On the east coast of Taiwan, the ocean waves come mostly from the east. Therefore, SAR-derived wave spectra can also be reliably used.

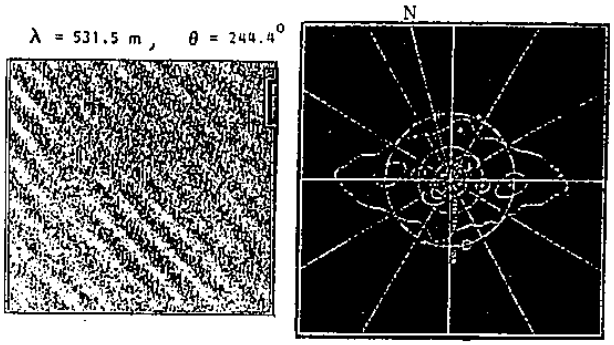

Figure 2. Alaska SAR Facility Wave Products of SAR spectrum from December 29, 1991 in the Gulf of Alaska at location P in Figure 4.

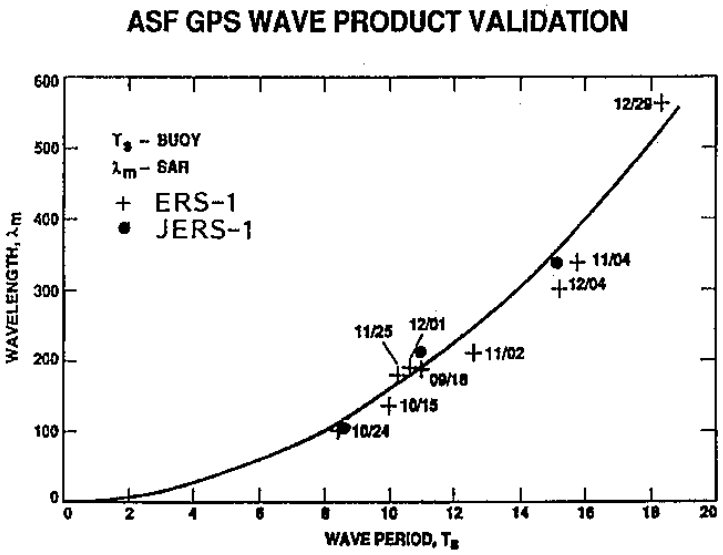

Figure 3. Wave Dispersion Relation from SAR Data and Buoy Data.

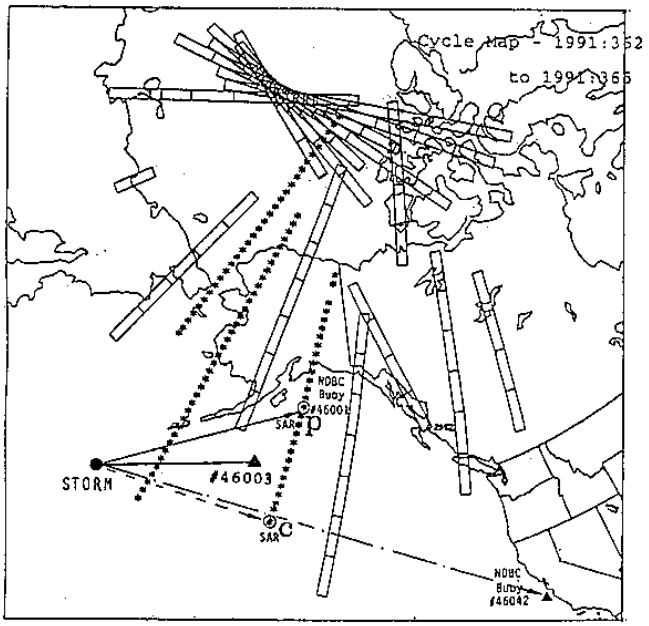

Figure 4. SAR Path of ERS-1 on December 29, 1991 over the Gulf of Alaska and the Bering Sea with Buoy Locations and Tracked Storm Area indicated.

3. Storm and Swell Evolution

Figure 4 shows the SAR path of ERS-1 on December 29, 1991 over the Gulf of Alaska and the Bering Sea with three NDBC buoy locations indicated (#46001, #46003, and #46042). Based on the SAR spectra from two SAR images (locations P and C) as indicated by circles in Figure 4, the storm can be tracked by tracing back from two swell propagation directions. An Alaska SAR Facility wave product (SAR spectrum) collected on December 29, 1991 in the Gulf of Alaska near NDBC buoy #46001 location is shown in Figure 2 (location P in Figure 4). This large swell system of 565 m wavelength propagated northeastward with a direction of 60 degree from the North. This swell system was also observed from NDBC buoy #46001 with peak frequency of 0.05 Hz (620 m) and the significant waveheight of 6 m at 2100 UTC on December 29, 1991 (Figure 5). Further down on the SAR path at location C, the SAR spectrum is derived and the swell wavelength was 390 m with a propagation direction of 85 degree from the North.

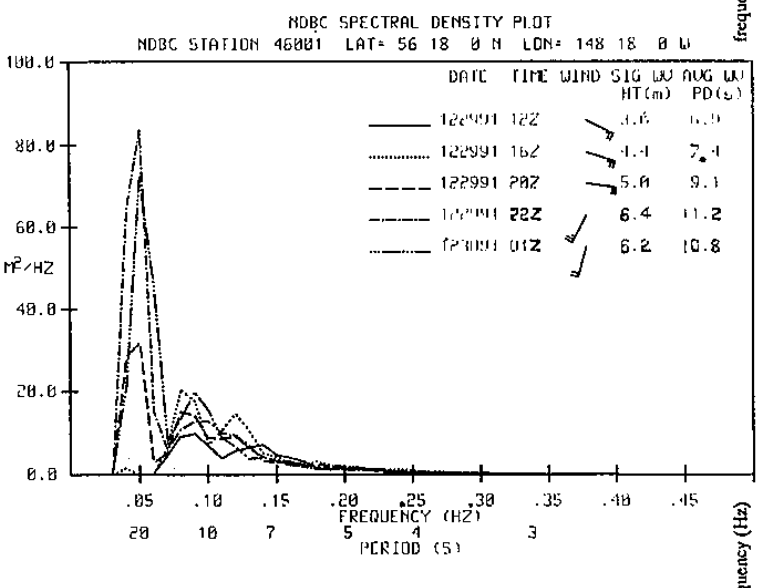

Figure 5. Wave Spectra from NDBC Station 46001 on December 29, 1991.

According to the surface synoptic weather charts, the storm (low pressure system) developed in the Bering Sea and began to move eastward at 00 UTC on December 27, 1991. At 00 UTC on December 28, the intensive storm had matured with center pressure of 954 mb and was moving toward the south of Aleutian Islands. The large and intense wave generation fetches on the southeast side of storm center were oriented northeastward. The storm had begun to weaken and its forward speed began to decrease by 00 UTC on December 29. The center of swell generation fetch is estimated at coordinate (45°N, 177°W). Contour plots of wave spectral evolution during December 27 to December 31, 1991 are shown in Figure 6a for buoy #46001, and Figure 6b for buoy #46003. Using the ridge-line approach, the time of long swell was approximately 00 UTC on December 28, 1991. Figure 7 shows swell spectral density time series during December 28 to December 31 for the NDBC buoy #46001 (solid line) and #46003 (dashed line). The swell system arrived at station 46001 at 2000 UTC, and arrived at station 46003 at 1000 UTC on December 29, 1991.

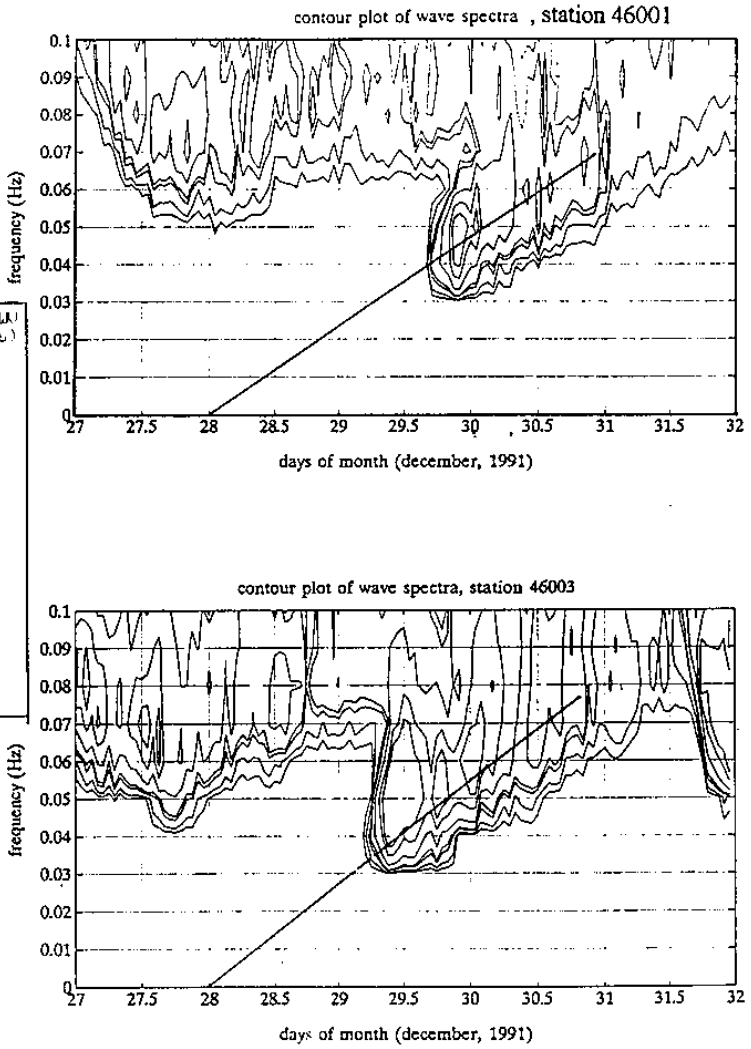

Figure 6. Contour Plots of Wave Spectra from (a) Station 46001, and (b) Station 46003 during December 27 to December 31, 1991.

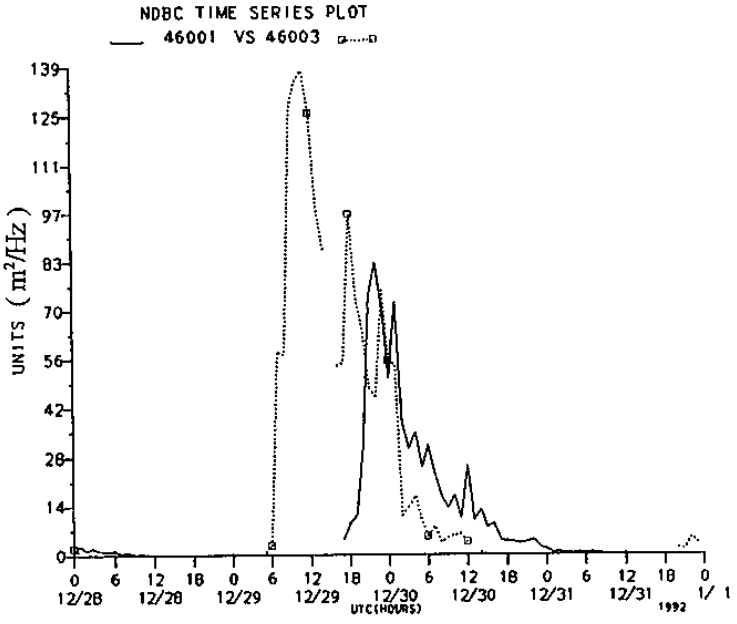

Figure 7. Time Series Plot of Peak Wave Spectral Density for Buoy #46001 (solid line), and Buoy #46003 (dashed line) during December 28 to December 31, 1991.

4. Wave Model and Analysis

Gonzalez et al. (1987) have shown that swell seem to obey the linear wave theory of propagation and do not seem to be affected by propagation through zones of steady wind. It is assumed that the waves originate from nearly a point source or a generation region sufficiently far away to be considered as nearly a point source. Swell (wavenumber k) generation is defined as that point when the deep water group velocity

$$C_g = (g\,k)^{1/2} \qquad (1)$$

exceeds the local wind speed component in the wave direction. Where g is the gravity constant. The wave then ceases to be forced by the wind and begins to propagate freely as swell. By assuming such swell system consists of free waves and is unaffected by other processes, such as wave-wave interaction and wave-current interaction, the swell directions at locations P and C can be checked with the linear wave model. Geometry of the idealized storm swell kinematic model is shown in Figure 8 with position of S(ϕ, λ) for the center of swell generation fetch. The great-circle distance s is given by (Snyder, 1987)

$$\sin(s/2) = [\sin^2(\phi_s/2-\phi_p/2)+\cos\phi_s\cos\phi_p\sin^2(\lambda_s/2-\lambda_p/2)]^{1/2} \qquad (2)$$

where s is the radian measure of the great-circle distance. The azimuth angle β_p of P, is found by combining two angles. The first angle θ_p is the internal angle subtended by two great circles-one that extends through S and P and the other that extends through P and C. The second angle θ_r is the azimuth angle from P to C (SAR path). Spherical geometry (Figure 9) then determines the following relationship:

$$\theta_p = \pi/2 - \cos^{-1}[(\cos l - \cos s \cos d)/(\cos s \cos d)] \qquad (3)$$

and

$$s = C_g\ (t_p - t_s) \qquad (4a)$$

$$l = C_g\ (t_c - t_s) \qquad (4b)$$

In these relationships, if the quantities of (ϕ, λ), C_g, and t_s are assumed known, then Equations (2-4) can be solved for the swell direction β and arrived time t_i for locations P and C.

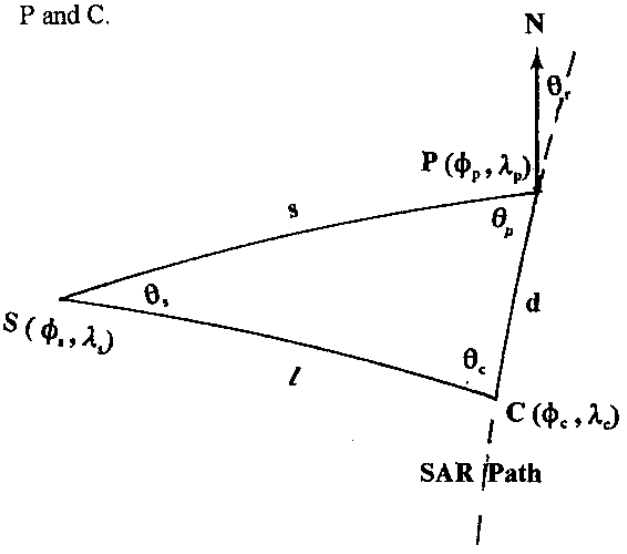

Figure 8. Diagram of the Geometry of the Idealized Storm Swell Kinematic Model. The Point S Represents the Center of Swell Generation Fetch, P and C are Points of SAR Imaging Locations.

5. Model Results

The positions of S, P and C are given by

$\phi_p = 56.2°$, $\phi_c = 46.6°$, $\phi_s = 45°$,
$\lambda_p = 149.8°$, $\lambda_c = 153.3°$, $\lambda_s = 177°$.

From Equation (2), the great-circle distances are found to be

d = 9.94° = 1100 km,
s = 20.4° = 2260 km,
l = 16.5° = 1835 km,

and the angles are

$\theta_p = 54.0°$, $\theta_c = 98.4°$, $\theta_s = 29.1°$, $\theta_r = 14°$,

The azimuth angles of P and C can be obtained as follows:

$\beta_p = 67.1°$, $\beta_c = 84.5°$,

which agree well with the results from SAR spectra of 60° for subscene P and 85° for subscene C.

The group velocity of a swell with wavelength of 565 m is approximately 53.4 km/hr. The distance between the storm and NDBC buoy #46001 is approximately 2260 km. Then, the time for this swell system traveled from the storm to the buoy location will be 42.3 hrs, which is consistent with 45 hrs between the estimated swell generation time (0000 UTC December 28) and SAR observation time (2100 UTC December 29). The distance between the storm and station 46003 is approximately 1722 km. The swell propagation time will be 31 hrs, which agrees well with the arrival time (0600 UTC December 29) at station 46003 as shown in Figure 6b. The eastern traveling swell system had a shorter wavelength of 388 m at station 46003. This maybe caused by the shorter fetch and the unfavorable generation direction which was not parallel to the storm isobar contours. The group velocity of 388 m swell is 44 km/hr, and the distance from the center of swell generation fetch to SAR imaging location C is approximately 1835 km. Thus, the time for this swell system to travel to position C will be 41.7 hrs, which is consistent with previous results.

Furthermore, by examining the directional spectral data from NDBC buoy #46042 near Monterey, California (Figure 9), the same swell system propagated through North Pacific Ocean and showed at 1000 UTC December 31, 1991 on the buoy data. The peak wave frequency is 0.05 Hz (620 m) and the propagation direction is 60° which is consistent with the estimated wavelength and direction.

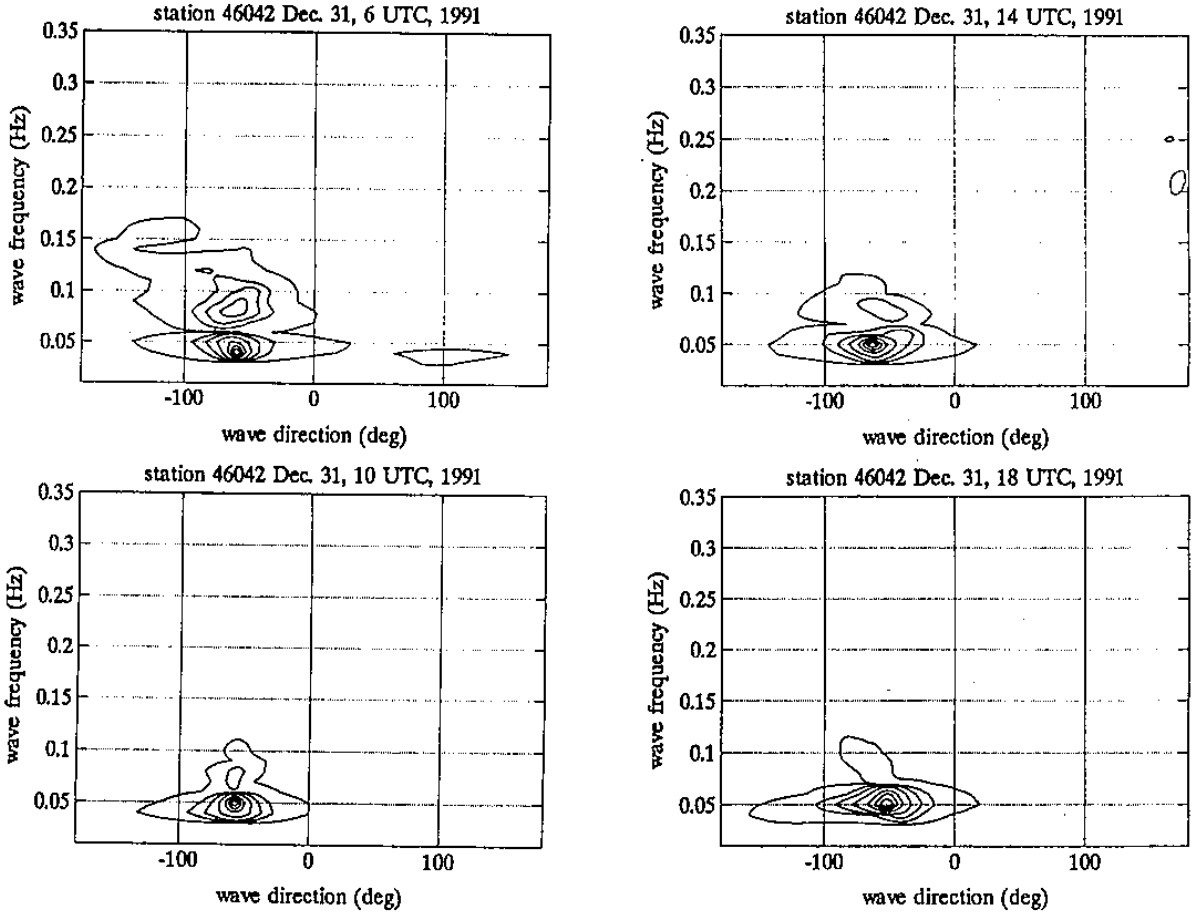

Figure 9. Directional Wave Spectra from Buoy #46042 near Monterey, California at 0600 UTC, 1000 UTC, 1400 UTC, and 1800 UTC on December 31, 1991.

6. Discussion

A simple kinematic model has been used in an analysis of a dominant swell system generated by storm observed by ERS-1 SAR and NDBC buoys in the Bering Sea. The results suggest that waves were generated 42 hrs before the SAR overpass, primarily in the east quadrant of the storm, at radii of several hundred kilometers. The generation time and area of the swell were estimated by using the traveling speed and wave direction from the buoys and SAR spectra. The estimated generation time and area were consistent with the location and the strength of the storm. By using the SAR spectra along the SAR path, a storm area can be tracked through swell propagation direction. The difference in the arrival times of the extremely high swells between the buoy stations and the SAR scenes along the coast clearly indicated the feasibility of the advanced warning of high swell. This application for storm tracking and coast watch could be crucial to the safety of offshore operations.

The coastal zone in Taiwan is a highly productive and dynamic environment. Because of the fast growth of industry, the storm surge is one of the major issues for environmental protection. Increasingly, coastal regions need reliable, high quality resource and environmental information from remote sensing to better manage this vital area. Remote sensing with repeated coverage is the most efficient method to monitor and study coastal protection. The tracking of swells generated by storm in the coastal zone is a major potential application for satellite data, especially for the SAR on RADARSAT with 500 km swath. The use of SAR-derived observations to track eddies, oil spills, surface temperature-related features, and river and estuarine plumes can also aid in the management of environment. Especially in subtropical and tropical regions, uniform sea surface temperatures and cloud cover preclude AVHRR measurements of surface structure, and obscure ocean color observations. The application of satellite data for coastal monitoring is highly recommended and requires government's sponsor and encouragement.

7. Acknowledgments

The authors wish to thank C. Y. Peng, and Y. Y. Chao for their valuable discussions and suggestions. GSFC work was supported by the National Aeronautics and Space Administration and Office of Naval Research.

8. References

Alpers, W. R., Ross, D. B. and C. L. Rufenach, On the delectability of ocean surface waves by real and synthetic aperture radar, J. Geophys. Res., 86, 6481-6498, 1981.

Gonzalez, F. I., Holt, B. M., and Tilley, D. G., The age and source of ocean swell observed in hurricane Josephine, Johns Hopkins Tech. Digest, 8, 94-99, 1987.

Hasselmann, K., Raney, R. K., Plant, W. J., Alpers, W., Shuchman, R. A., Lyzenga, D. R., Rufenach, C. L. and M. J. Tucker, Theory of synthetic aperture radar ocean imaging: A MARSEN view, J. Geophys. Res., 90, 4659-4686, 1985.

Liu, A. K., and C. Y. Peng, Ocean wave study using SAR, Satellite Remote Sensing of Oceanic Environment, I. S. F. Jones, R. W. Stewart, and Y. Sugimori, Editors, Seibutsu Kenkyusha Press, 1993.

Liu, A. K., C. Y. Peng, and J. D. Schumacher, Wave-current interaction study in the Gulf of Alaska for detection of eddies by SAR, J. Geophys. Res., 99, 10075-85, 1994.

Peng, C. Y., and A. K. Liu, SAR observations of interaction of ocean swell and Semidi Islands in the Gulf of Alaska, International J. Rem. Sens., 16, 1249-60, 1995.

Snyder, J. P., Map projections-a working manual, U.S. Geological Survey Professional Paper 1395, U.S. GPO 383pp, 1987.

WAMDI Group, The WAM model-a third generation ocean wave prediction model, J. Phys. Oceanogr., 18, 1775-1810, 1988.